Electronic Supplementary Material (ESI) for ChemComm.

ELECTRONIC SUPPLEMENTARY INFORMATION

Design of High-Performance NIR-II Nanoprobe by Steric Regulation for in vivo Vasculature and Tumor Imaging

Yu Wang,# Yuxin Duan,# Chenxing Gong, Yuhang Li, Meilin Xu, Miao Liu, Wenxu Liu,* Xiaole Zhou,* and Leyu Wang*

State Key Laboratory of Chemical Resource Engineering, Beijing Advanced Innovation Center for Soft Matter Science and Engineering, Beijing University of Chemical Technology, Beijing 100029, P. R. China.

E-mail: lywang@mail.buct.edu.cn; zhouxiaole@buct.edu.cn; liuwenxu@buct.edu.cn

# These authors contributed equally.

Contents:

1. Representative NIR dyes

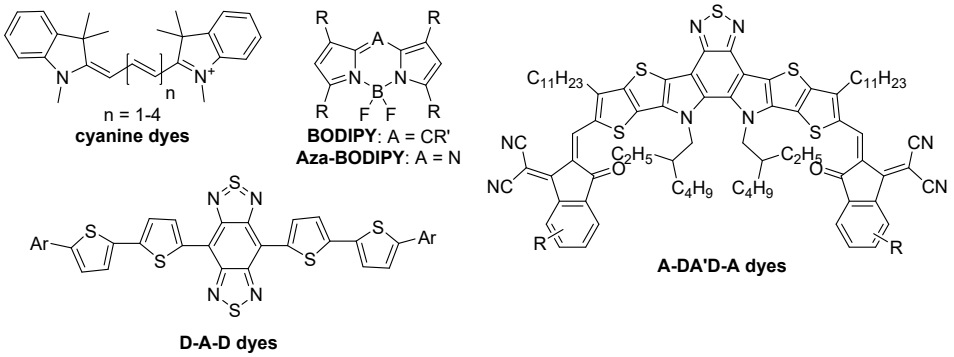

Figure S1. Some well-studied NIR dyes.

2. Further explanation for the effect of norbornyl group

The strong tendency of A-DA'D-A dye molecules to form π-π stacking interactions with neighboring molecules via the terminal A groups has been extensively elucidated, as demonstrated by the analysis of single crystal structures. This underscores the pivotal role played by the terminal groups in governing the molecular packing arrangements.[1,2]

The single crystal of the norbornyl annulated 1,1-dicyanomethylene-3-indanone (CBIC) was retrieved from CCDC database (CCDC number: 2060724).[3,4] It can be seen from Figure S2 that CBIC exhibits unique exo conformation with the methylene bridge (C-7) of the norbornyl moiety apparently stretches out of the conjugated system. This conformation, validated by DFT calculations, hinders terminal-to-terminal intermolecular interactions on the norbornyl side, thereby mitigating the aggregation of SM-16. This structural feature is anticipated to enhance the quantum yield in the solid state.

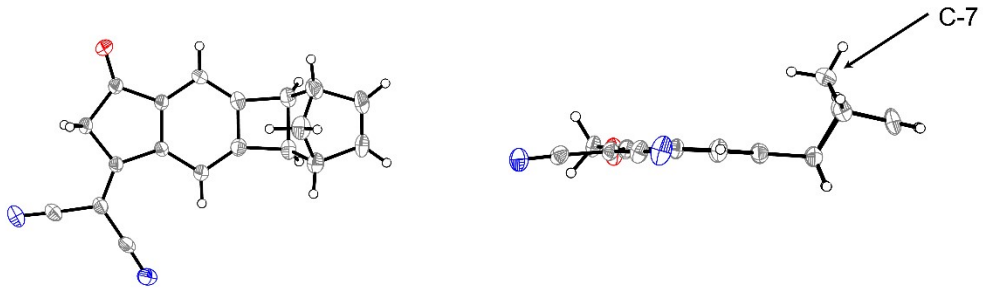

Figure S2. The single crystal diagram of SM-16 terminal group.

3. Materials and general methods

3.1. Chemicals

All of the chemicals and solvents used for synthesis were obtained from commercial suppliers and used directly without further purification. F127 was purchased from Laysan Bio, Inc. Phosphate buffer solution (PBS), dulbecco's modified eagle medium (DMEM) and trypsin were purchased from M&C Gene Technology. Methyl thiazolyltetrazolium (MTT) was obtained from Amresco Inc. Fetal calf serum (FBS) was obtained from Hangzhou Sijiqing Bio-engineer Materials Ltd. Deionized (DI) water was used throughout all experiments.

3.2. Instrumentation

DLS particle size analysis was carried out using a Zetasizer Nano-ZS90 zeta and size analyzer from Malvern. Nuclear magnetic resonance (NMR) spectra were recorded on a AVANCE III HD 400 MHz NMR spectrometer (400 MHz for ^{1}H, referenced to TMS at δ = 0.00 ppm). TEM images were acquired by using a JEOL JEM-1200EX (200 KV). UV–vis–NIR spectra were measured on a Shimadzu UV-3600 spectrometer. PL spectra and the absolute photoluminescence quantum yield were recorded on an Edinburgh instruments FLS980 (excitation source: 808 nm laser; signal detection: a liquid nitrogen cooled InGaAs diode detector).

3.3. Synthesis.

Compounds SM-16 and Y6 were synthesized according to the literature.[5,6]

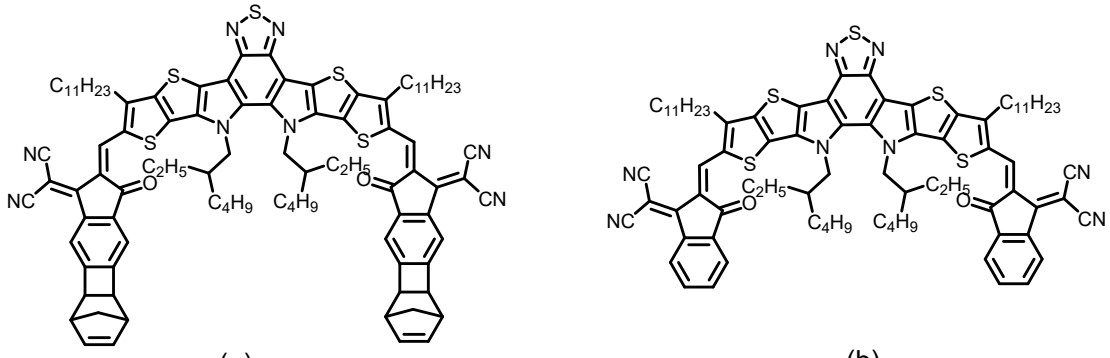

Figure S3. The Structure of **SM-16** and **Y6**.

4. Theoretical calculations

Theoretical calculations were conducted using the Gaussian 16 program at the B3LYP/6-31G(d) level to determine the optimal molecular geometries and distribution of frontier molecular orbitals for SM-16 and Y6.

To simplify, methyl groups were substituted for the long alkyl chains on the DA'D cores. As shown in Figure S4, both dye molecules exhibit slightly twisted backbones, with an N-C-C-N dihedral angle of approximately 10° due to the alkyl groups attached to the nitrogen atoms, effectively preventing dye over-aggregation.[7] Furthermore, both dye molecules display a similar distribution of frontier orbitals. Specifically, the highest occupied molecular orbital (HOMO) of both dyes is localized on their central electron-rich core, while the lowest unoccupied molecular orbital delocalizes across the entire conjugated skeletons. The slightly shallower HOMO and LUMO energy levels of SM-16 compared to Y6 can be attributed to the weak electron-donating ability of the terminal norbornyl groups.

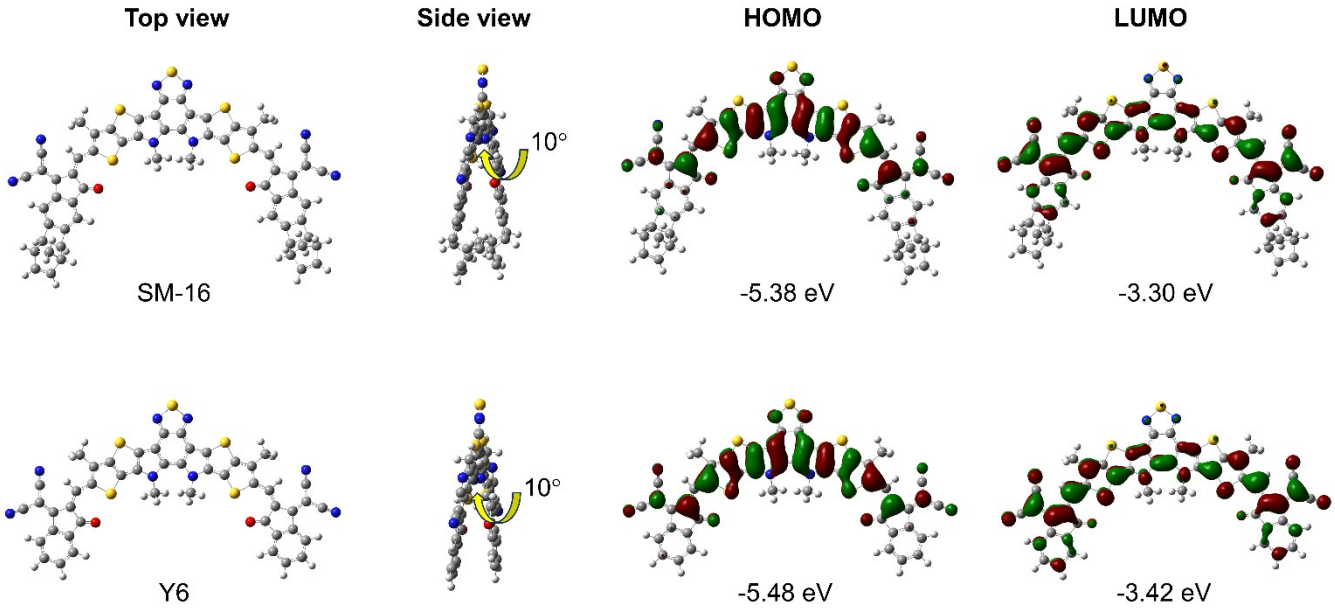

Figure S4. The optimal molecular geometries and distribution of frontier molecular orbitals for SM-16 and Y6.

5. Preparation of the nanoparticles.

A series of **SM-16 NPs** with different loading ratios was prepared as follows: F127 (10 mg) and **SM-16** (0.1, 0.2, 0.4, 0.8 and 1.2 mg) were dissolved in 200 μL of dichloromethane, and the solution was added to 10 mL of ultrapure water via a micro-syringe. After that, the obtained mixture was treated with ultrasonication in ice bath for 2 min and stirred at 40 ºC for 1 h to remove the organic solvent. The solution was firstly centrifuged at 3000 rpm for 10 min and the supernatant was retained as **SM-16 NPs**. **Y6 NPs** is prepared and optimized by the same process as **SM-16 NPs**.

6. Optimization of the ratio of SM-16 and Y6 to F127.

Then fluorescence intensities in NIR-II region (1025 nm) of **SM-16 NPs** and **Y6 NPs** with loading ratios were measured, and the results were recorded in **Figure S-S1** (plots of fluorescence intensity *vs* dye amounts).

TEM images of **SM-16 NPs** were also measured, and some representative images were shown in the **Figure S-S2**.

SM-16 NPs showed strongest fluorescence when **SM-16**:F-127 = 0.4:10, but the TEM result indicated the NPs had poor morphology at that ratio. While at the ratio of **SM-16**:F-127 = 0.8:10, **SM-16 NPs** exhibited both good fluorescence and uniform morphology, so we choose 0.8:10 as the optimal condition. For Y6, it also showed remarkable fluorescence at the ratio of Y6:F-127 = 0.8:10, so we choose that ratio to minimize the variable in comparation.

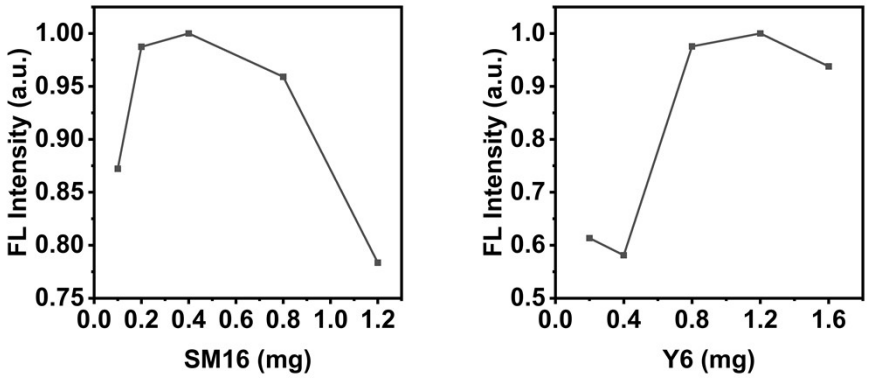

Figure S-S1. The change of fluorescence intensity in NIR-II region (1025 nm) of SM16 NPs (left) and Y6 NPs (right) at different molecular concentrations.

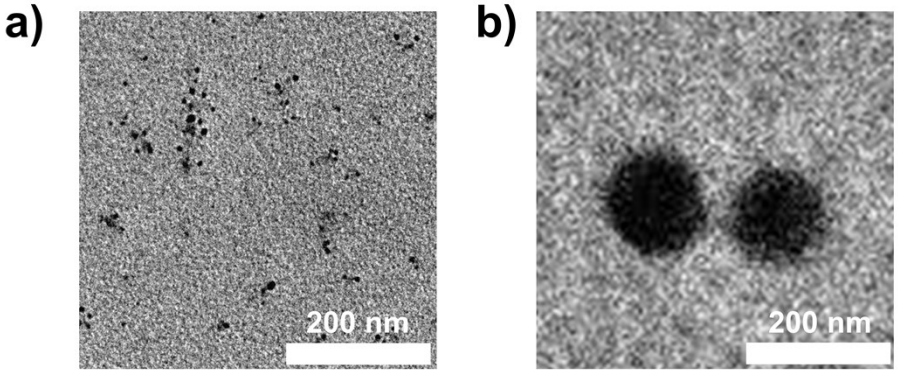

Figure S-S2. The TEM images of SM16 NPs. a) SM16 0.4 mg, F127 10 mg; b) SM16 0.8 mg, F127 10 mg.

7. Determination of encapsulation efficiency.

*Calibration curve for absorbance of **SM-16***: **SM-16** was dissolved in toluene and separately diluted to concentration of 2, 4, 6, 8, 10, 12, 14 and 16 μmol/L, and the absorbance at the corresponding molecule concentration was obtained using UV spectrophotometer and utilized to generate the calibration curve (**Figure S5-S6**). Compared with the main absorption peak at 696 nm, the absorption peak at 574 nm might follow the linear trend over a larger concentration range. Therefore, calibration curve was obtained through the absorbance of **SM16** molecule at 574 nm (**Figure S6**).

The encapsulation efficiency of **SM-16** in NPs was determined by using UV spectrophotometer measurement after disassembling the micelles, according to the absorbance-concentration plot in **Figure S5-S6**.

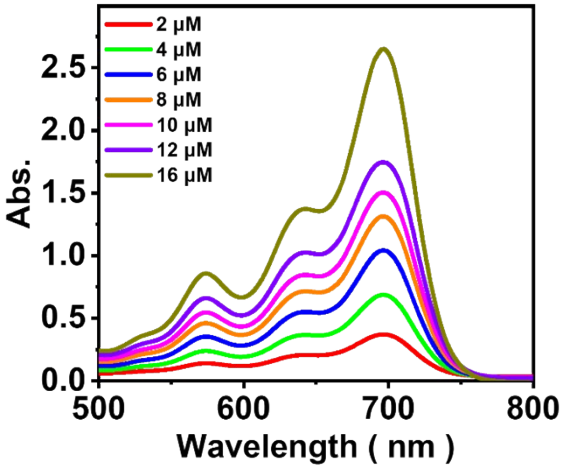

Figure S5. The different absorption spectra of **SM-16** in toluene with increasing concentrations.

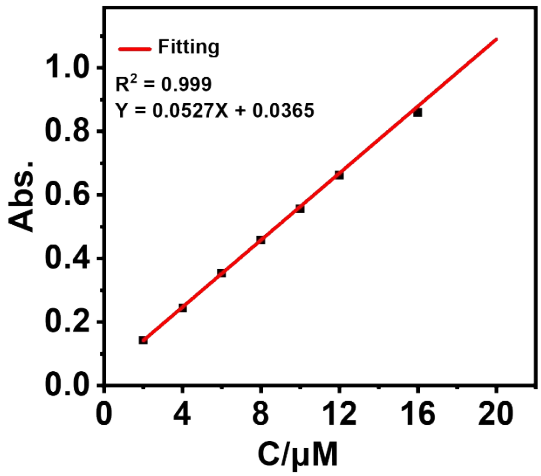

Figure S6. Absorbance of **SM16** molecule at 574 nm plotted as a function of the concentration of **SM-16** in toluene based on the result of **Figure S5**.

8. Colloidal stability determination.

A solution of SM-16 NPs (10 μM in PBS) were incubated at 37 °C for 40 days. During that time, the colloidal diameters of SM-16 NPs were measured at the same time in the selected days.

9. Photostability detection.

A continuous photo-irradiation experiment was performed to evaluate the photostability of SM-16 NPs, with free ICG as a comparation. In detail, 2.0 mL aqueous SM-16 NPs solution (concentration of SM-16: 2 μM) was continuously irradiated for 30 min with an 808 nm laser at a power of 0.3 $W \cdot cm^{-2}$. The photostability of

SM-16 NPs was determined by measuring the fluorescence emission intensity, compared with that of free ICG.

10. Cell culture.

4T1 cell were maintained as monolayer cultures in DMEM at 37 ºC in 5% CO_2 incubator, the mediums were supplemented with 10% FBS and 1% penicillin/streptomycin. The cells were cultured until confluence was reached before each experiment.

11. Cytotoxicity measurement.

$5*10^4$ 4T1 cell seeded in 96-well plates were pre-cultured for 24 h, and then the culture medium was replaced by medium containing SM-16 NPs, and the concentrations of SM-16 in the plates were 0.0, 10.0, 30.0, 60.0, 90.0, 120.0 μM respectively. After 4 h incubation, the culture medium containing SM-16 NPs was removed, and the cells were washed with PBS solution for three times. Then new culture medium without SM-16 NPs was added, and the cells were incubated for another 24 h. Finally, the cell viabilities were determined by MTT assay, and the results were presented as average ± SD (n = 5).

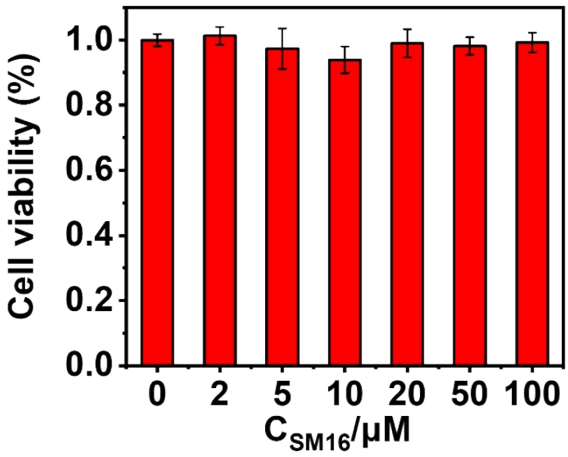

Figure S7. The cytotoxicity of **SM-16 NPs** being determined by MTT assay. Error bars indicate standard errors of quintuple tests.

12. Animal experiments.

All experiments involving animals were approved and performed in accordance with the guidelines of the Institutional Animal Care and Use Committee (IACUC) of the China-Japan Friendship Hospital and Beijing University of Chemical Technology. All the mice were housed groupedly in cages with woodchip bedding and the standard supply of water and fodder. Animal experiments were conducted in 5-week-old BALB/C female mice purchased from SPF Biotechnology Co., Ltd (Beijing, China). Animal experiments were conducted in 5-

week-old BALB/C female mice. The mice were subcutaneously injected with 1×10^6 4T1 cells each mouse on the right leg. After 10 days, a solid tumor about 300 mm^3 formed during the period.

13. NIR-II fluorescence imaging of vasculature.

The solution of SM16 NPs (400 μmol/L,100 μL) and ICG (400 μmol/L, 100 μL) were intravenously injected into the 5-week-old BALB/C nude female mice through the tail vein, respectively. After ten minutes, the mice were anesthetized with isoflurane to image the vasculature.

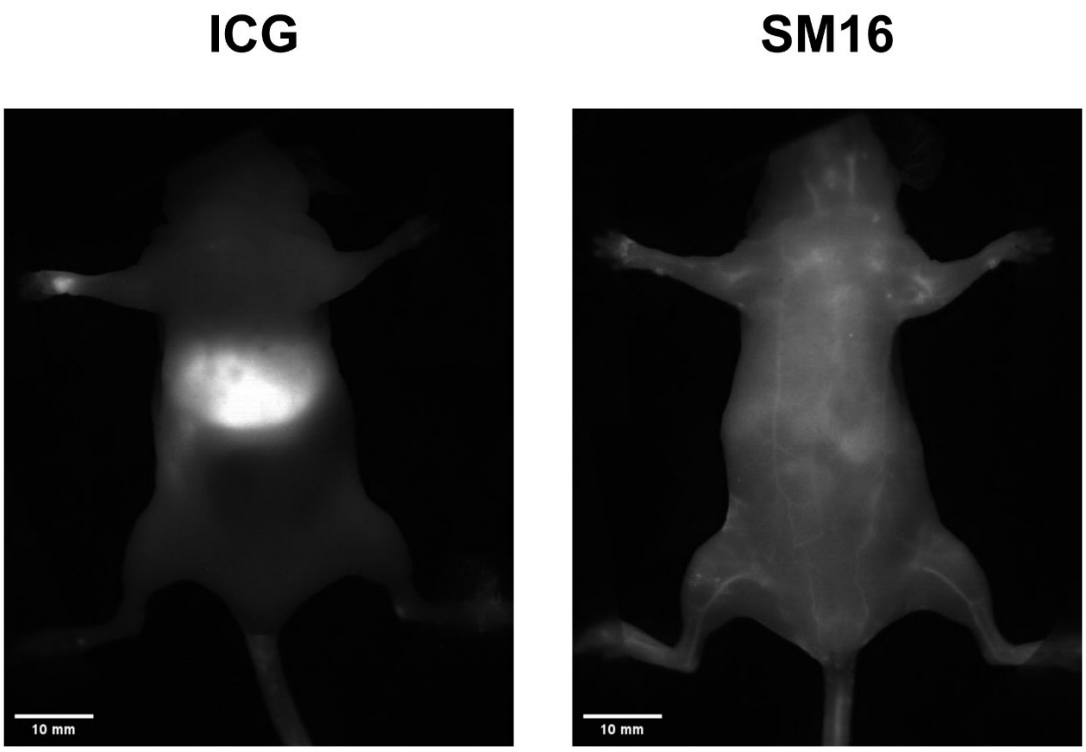

Figure S8. Images of mouse right hindlimb vasculature after intravenous injection of free ICG (left) and **SM-16 NPs** (right).

14. NIR-II fluorescence imaging of tumors.

Firstly, the fur surrounding the tumor was removed from the tumor-bearing mice. Then, 100 μL solution of SM-16 NPs (SM-16 concentration: 2 mmol/L) was intravenously injected into the mice through the tail vein. After that, the mice were anesthetized with isoflurane to imaging the tumor at indicated time points.

15. Table S1. Photophysical properties of SM-16 and Y6

Table S1. Photophysical properties of SM-16 and Y6.

Materials	Solvent	λ_{abs} [nm][(a)]	ε [L·cm^{-1}·mol^{-1}][(b)]	λ_{em} [nm][(c)]	Φ (%)[(d)]	Brightness [L·cm^{-1}·mol^{-1}]
SM-16	**Toluene**	**696**	**1.1×10^5**	**768**	**20.33**	**2236.3**
SM-16 NPs	**PBS**	**776**	**6.7×10^4**	**868**	**0.2**	**134**
Y6	**Toluene**	**699**	**0.50×10^5**	**741**	**n. d.**	**n. d.**
Y6 NPs	**PBS**	**772**	**6.2×10^4**	**866**	**0.09**	**55.80**

(a) Absorption peak. (b) Molar absorptivity of the corresponding absorption peak. (c) Fluorescence emission peak. (d) Absolute photoluminescence quantum yield. n. d. = not determined.

Reference

1 G. Li, X. Zhang, L. O. Jones, J. M. Alzola, S. Mukherjee, L. Feng, W. Zhu, C. L. Stern, W. Huang, J. Yu, V. K. Sangwan, D. M. DeLongchamp, K. L. Kohlstedt, M. R. Wasielewski, M. C. Hersam, G. C. Schatz, A. Facchetti and T. J. Marks, *J. Am. Chem. Soc.*, 2021, **143**, 6123–6139.

2 J. Hou, O. Inganäs, R. H. Friend and F. Gao, *Nat. Mater.*, 2018, **17**, 119–128.

3 C. R. Groom, I. J. Bruno, M. P. Lightfoot and S. C. Ward, *Acta Crystallogr. Sect. B Struct. Sci. Cryst. Eng. Mater.*, 2016, **72**, 171–179.

4 H. Lu, H. Jin, H. Huang, W. Liu, Z. Tang, J. Zhang and Z. Bo, *Adv. Funct. Mater.*, 2021, **31**, 2103445.

5 J. Yuan, Y. Zhang, L. Zhou, C. Zhang, T. Lau, G. Zhang, X. Lu, H. Yip, S. K. So, S. Beaupré, M. Mainville, P. A. Johnson, M. Leclerc, H. Chen, H. Peng, Y. Li and Y. Zou, *Adv. Mater.*, 2019, **31**, 1807577.

6 H. Lu, W. Liu, H. Jin, H. Huang, Z. Tang and Z. Bo, *Adv. Funct. Mater.*, 2022, **32**, 2107756.

7 J. Yuan, Y. Zhang, L. Zhou, G. Zhang, H.-L. Yip, T.-K. Lau, X. Lu, C. Zhu, H. Peng, P. A. Johnson, M. Leclerc, Y. Cao, J. Ulanski, Y. Li and Y. Zou, *Joule*, 2019, **3**, 1140–1151.